Biosensors and Bioelectronics 249 (2024) 116046

Contents lists available at ScienceDirect

Biosensors and Bioelectronics

journal homepage: www.elsevier.com/locate/bios

CRISPR/Cas9-mediated SERS/colorimetric dual-mode lateral flow platform combined with smartphone for rapid and sensitive detection of *Staphylococcus aureus*

Junfeng Wang [a,b,1], Han Jiang [a,1], Yuhong Chen [b], Xiaofan Zhu [a], Qian Wu [c], Wei Chen [c,***], Qihong Zhao [a], Jie Wang [b,**], Panzhu Qin [a,*]

[a] Department of Nutrition and Food Hygiene, School of Public Health, Anhui Medical University, Hefei, 230032, Anhui, PR China
[b] School of Pharmacy, Anhui Medical University, Hefei, 230032, Anhui, PR China
[c] School of Food and Biological Engineering, Hefei University of Technology, Hefei, 230009, Anhui, PR China

ARTICLE INFO

Keywords:
CRISPR/Cas9
Lateral flow strip
Colorimetry
SERS
S. aureus

ABSTRACT

Pathogenic bacteria infections pose a significant threat to global public health, making the development of rapid and reliable detection methods urgent. Here, we developed a surface-enhanced Raman scattering (SERS) and colorimetric dual-mode platform, termed smartphone-integrated CRISPR/Cas9-mediated lateral flow strip (SCC-LFS), and applied it to the ultrasensitive detection of *Staphylococcus aureus* (*S. aureus*). Strategically, functionalized silver-coated gold nanostar (AuNS@Ag) was prepared and used as the labeling material for LFS assay. In the presence of *S. aureus*, target gene-induced amplicons can be accurately recognized and unwound by the user-defined CRISPR/Cas9 system, forming intermediate bridges that bind many AuNS@Ag to the test line (T-line) of the strip. As a result, the T-line was colored and a recognizable SERS signal was obtained using a smartphone-integrated portable Raman spectrometer. This design not only maintains the simplicity of visual readout, but also integrates the quantitative capability of SERS, enabling the user to flexibly select the assay mode as needed. With this method, *S. aureus* down to 1 CFU/mL can be detected by both colorimetric and SERS modes, which is better than most existing methods. By incorporating a rapid extraction procedure, the entire assay can be completed in 45 min. The robustness and practicality of the method were further demonstrated by various real samples, indicating its considerable potential toward reliable screening of *S. aureus*.

1. Introduction

Pathogenic bacterial infections are a major public health threat, causing more than 15 million deaths annually (Cesewski and Johnson, 2020). Thereinto, *Staphylococcus aureus* (*S. aureus*) is a common pathogen that can induce skin infections and even extremely fatal diseases (Abbaspour et al., 2015). With the widespread use of traumatic surgery and organ transplantation in recent years, clinical infections caused by *S. aureus* have been increasing (Surewaard et al., 2016). The high morbidity and mortality of *S. aureus* infection makes it the leading cause of infection-related deaths worldwide (Bai et al., 2022). Currently, the gold standard for pathogen detection relies on bacterial cultures and biochemical identifications, which provide detailed information on infectious agents (Fu et al., 2021). However, in emergency situations that require timely test conclusions, alternative methods are urgently needed to avoid the extraordinarily long turnaround times involved in culture techniques.

Lateral flow strip (LFS) is a paper-based device that can be operated by untrained personnel (Sena-Torralba et al., 2022; Zhang et al., 2021a). Due to its portability, short turnaround time, and ability to isolate patients timely, many immunoassay-based LFSs have been developed for pathogen detection (Dong et al., 2023; Zhang et al., 2023). However, most of these strategies are limited by low sensitivity. Recently, advances in nucleic acid amplification and clustered regularly interspaced

* Corresponding author.
** Corresponding author.
*** Corresponding author.
E-mail addresses: chenweishnu@163.com (W. Chen), wangjienar@163.com (J. Wang), 15205519023@163.com, 2021500037@ahmu.edu.cn (P. Qin).
[1] These authors contributed equally to this research.

https://doi.org/10.1016/j.bios.2024.116046
Received 26 November 2023; Received in revised form 9 January 2024; Accepted 16 January 2024
Available online 17 January 2024

short palindromic repeats (CRISPR)/Cas technology have fueled the development of LFS as a versatile point-of-care testing tool (Yan et al., 2022; Zhang et al., 2021b). CRISPR-based LFS employs target analyte-induced preamplification such as recombinase polymerase amplification (RPA) to activate the trans-cleavage activity of Cas12a or Cas13a, providing excellent sensitivity (Chen et al., 2020b; Lu et al., 2022; Zhou et al., 2022b). Nevertheless, the trans-cleavage activities of Cas12a and Cas13a require an additional 30–60 min (Zhou et al., 2022a) and may be activated by non-target factors (Jiang et al., 2023). Unlike Cas12a and Cas13a, Cas9 has no trans-cleavage activity and can accurately recognize double-stranded DNA (dsDNA) with the help of single-guided RNA (sgRNA) (Balderston et al., 2021). In view of this, and considering that the amplification efficiency of RPA is sufficient for sensitive detection of pathogen, our recent works focused on utilizing Cas9 to improve the anti-interference of RPA-based LFS (Wang et al., 2022; Zhu et al., 2023). In this regard, the lack of quantitative capability seems to be the main shortcoming limiting the practical application of this strategy.

Recently, applying nanoscience to build engineered biosensors has led to significant progress in rapid diagnostics. Combining LFS with diverse nanomaterials not only retained the simplicity of visual readout in colorimetric mode, but also integrated the quantitative capabilities in fluorescence, surface enhanced Raman scattering (SERS), or electrochemical modes, enhancing the overall resilience of the assay (Cheng et al., 2023; Li et al., 2023; Liang et al., 2022; Preechakasedkit et al., 2023). Thereinto, SERS is a vibrational spectroscopy technique that can enhance the Raman signal of molecules by 10^{10}–10^{11} folds by noble metals or hybridized nanomaterials (Wang et al., 2021), showing great promise for point-of-care signal amplification and quantitative analysis (Zhu et al., 2020). Inspired by these works, we here proposed a SERS/colorimetric dual-mode platform, called smartphone-integrated CRISPR/Cas9-mediated LFS (SCC-LFS). As shown in Fig. 1A, the Raman reporter 4-aminothiophenol (4-ATP) was modified in the gap between gold nanostar (AuNS) and silver (Ag) shell and on the surface of Ag shell. Notably, we chose AuNS rather than conventional gold nanoparticle (AuNP) because multibranched AuNS have a stronger SERS sensitizing ability than spherical AuNP (Su et al., 2021). The Ag-coated AuNS (AuNS@Ag) was conjugated with a thiolated DNA probe to form AuNS@Ag-probe. In the presence of *S. aureus*, the DNA templates were first collected from the sample and then subjected to RPA using biotin-labeled forward primer (biotin-FP) and unlabeled reverse primer (RP) (Fig. 1B). The obtained biotin-labeled amplicons (^{Biotin}amplicon) contain a protospacer adjacent motif (PAM) site and a binding region and can therefore be recognized by Cas9/sgRNA. This resulting the formation of ^{Biotin}amplicon-Cas9/sgRNA complex with concomitant release of the 20-nt non-complementary strand. The non-complementary strand of amplicon could bind to AuNS@Ag-probe, forming ^{Biotin}amplicon-Cas9/sgRNA-AuNS@Ag complex (Fig. S1). When this mixture was loaded onto the strip and moved toward the direction of absorbent pad, the formed complex can be captured by streptavidin (SA) on the T-line (Fig. 1C), inducing a visible color signal. Meanwhile, the accumulation of AuNS@Ag-probe on the T-line produced a SERS signal that can be measured by a smartphone-integrated Raman spectrometer (Fig. S2). Notably, the control probe (CP) pre-modified on the C-line is partially complementary to the thiolated DNA probe and thus can trap AuNS@Ag-probe regardless of the presence or absence of *S. aureus*.

2. Materials and methods

More information is provided in the Supporting **Information**.

3. Results and discussion

3.1. Characterization of AuNS@Ag

The morphologies of AuNS with 4–6 sharp branches were first characterized by Transmission Electron Microscope (TEM) (Fig. 2A).

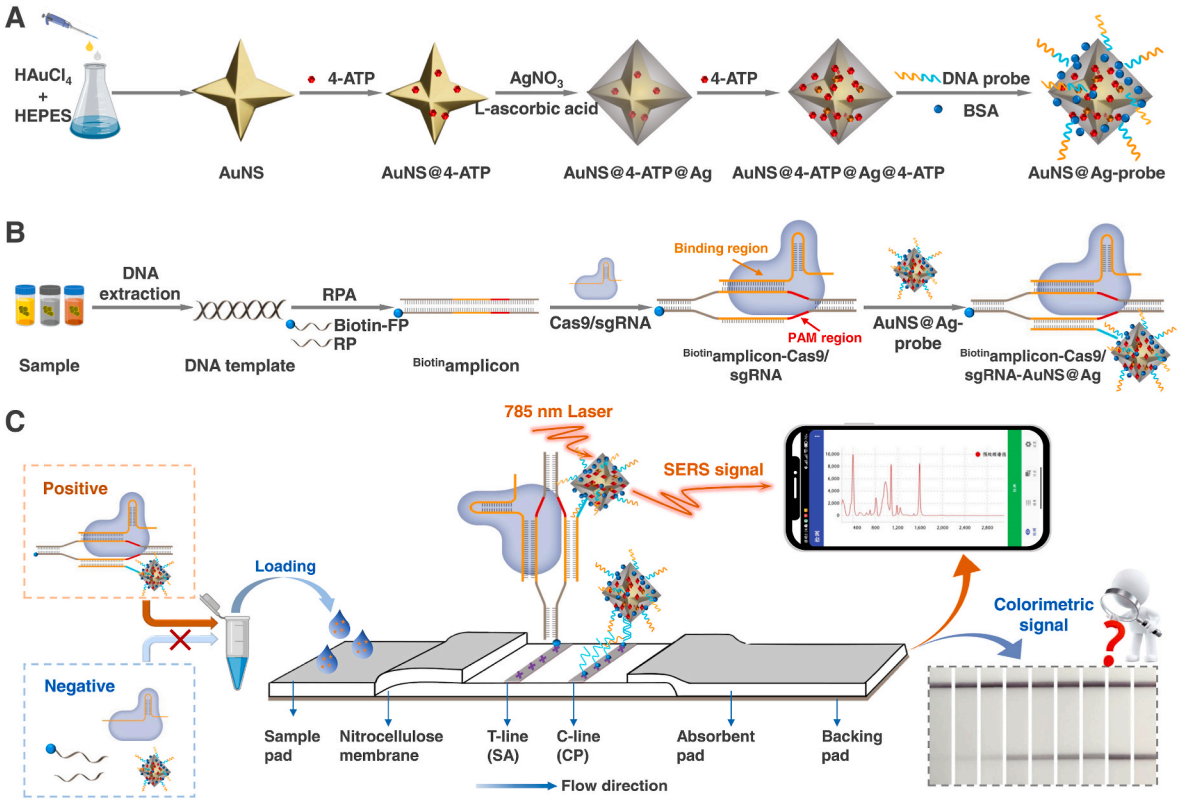

Fig. 1. Schematic of SCC-LFS for *S. aureus* assay.

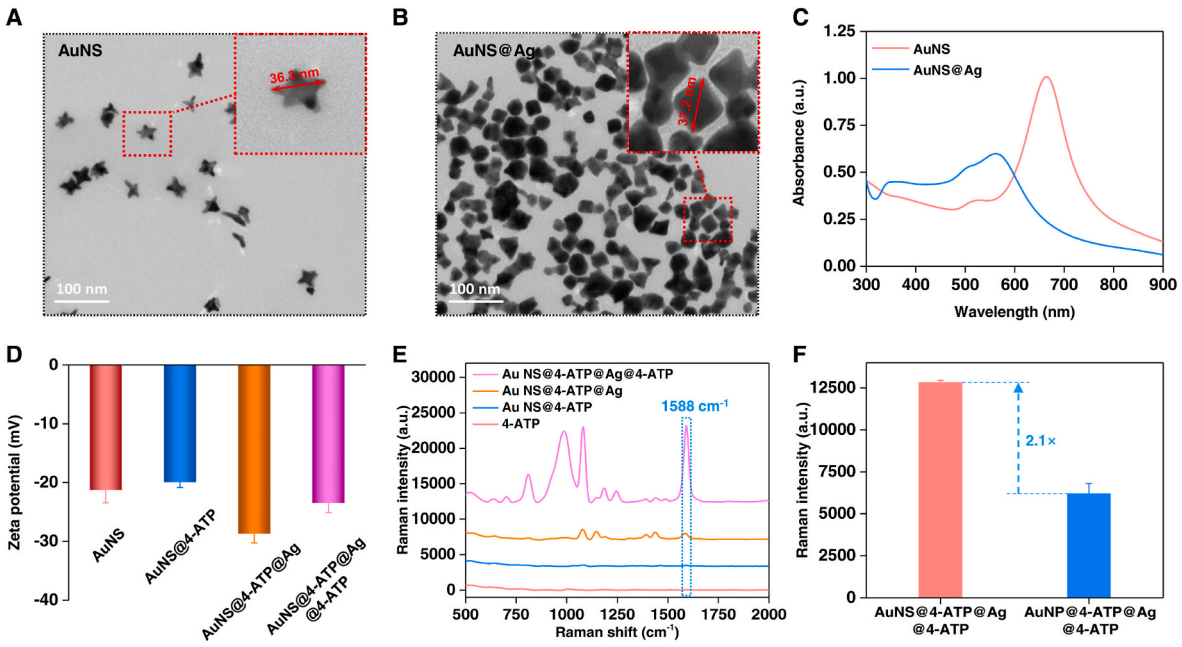

Fig. 2. (A–B) TEM images of AuNS and AuNS@Ag, respectively. **(C)** UV–vis spectra of AuNS and AuNS@Ag. **(D)** Zeta potentials of AuNS, AuNS@4-ATP, AuNS@4-ATP@Ag, and AuNS@4-ATP@Ag@4-ATP. **(E)** Raman analysis of 4-ATP, AuNS@4-ATP, AuNS@4-ATP@Ag, and AuNS@4-ATP@Ag@4-ATP. **(F)** Comparison of AuNS@4-ATP@Ag@4-ATP with AuNP@4-ATP@Ag@4-ATP. Error bars represent mean ± SD.

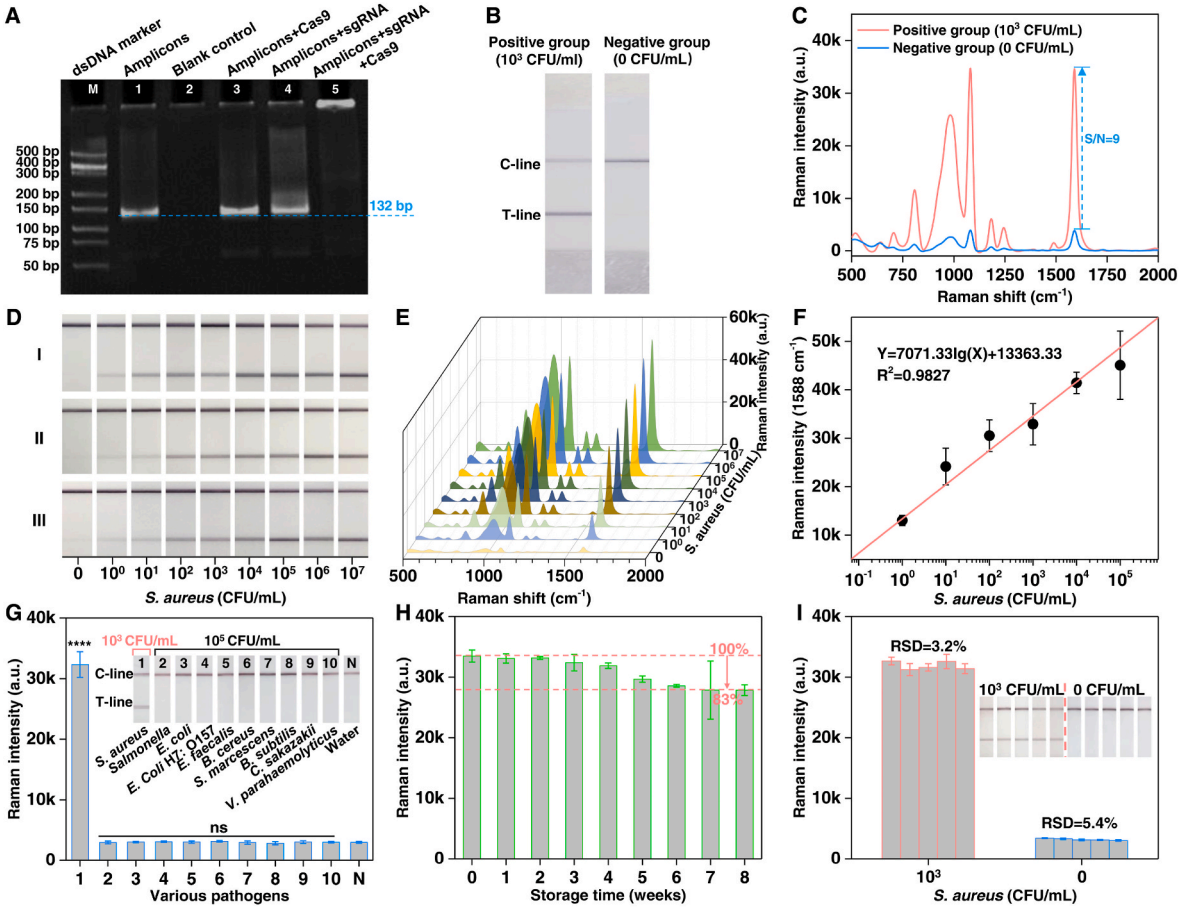

Fig. 3. (A) Electrophoresis analysis of various combinations. **(B)** LFS assay of the amplification products. **(C)** The corresponding Raman responses of (B). **(D)** LFS assay of *S. aureus* with various concentrations. **(E)** Raman responses of SCC-LFS to various *S. aureus* concentrations. **(F)** The plotted linear relationship between Raman intensity and *S. aureus* concentration (1–10^5 CFU/mL). **(G–I)** are the results of specificity, stability and reproducibility tests, respectively. The inset shows the corresponding LFS images. Error bars represent mean ± SD. ****, $P < 0.0001$; ns, not significant.

After Ag deposition, the concave sites of the star-shaped structure were filled with Ag shells to form AuNS@Ag (Fig. 2B), which was further confirmed by the corresponding EDS mapping analysis (Fig. S3). The UV–vis absorption spectrum of AuNS showed clearly absorption peaks at 522 nm and 705 nm (Fig. 2C), which corresponded to the transverse plasmon resonance of the branch and the longitudinal plasmon resonance between the neighboring branches, respectively (Su et al., 2011). The formation of Ag shell led to an increased absorption in the range of 360–600 nm due to the Au branches being buried in the Ag polyhedral (Zhao et al., 2019). Meanwhile, the absorption peak of AuNS at 705 nm disappeared with Ag coating, which could be attributed to the high-energy Ag peak masking the longitudinal resonance peak of the Au branches (Zhao et al., 2019). As depicted in Fig. 2D, the zeta potential of AuNS changed from −21.4 to −20.1 mV after binding to the positively charged 4-ATP. Upon Ag coating, the potential of particles became −28.8 mV. This makes sense because the large number of acid radical ions remaining on the surface of Ag shell made it negatively charged (Monga and Pal, 2015). With the binding of the second layer of positively charged 4-ATP, the potential changed to −23.6 mV. The results of Raman analysis in Fig. 2E showed that 4-ATP-adsorbed on the surface of AuNS given a weak Raman signal, which was then enhanced by the Ag shell. Continued modification of 4-ATP on the Ag shell resulted in a substantial enhancement of the Raman signal. Referring to a reported method (Trinh and Yoon, 2022), we calculated a SERS enhancement factor (EF) of 1.84×10^8 for AuNS@Ag. For comparison, we synthesized 4-ATP-modified Ag-coated AuNP (AuNP@4-ATP@Ag@4-ATP). As shown in Fig. 2F, the Raman signal of AuNS@4-ATP@Ag@4-ATP was about 2.1 times that of AuNP@4-ATP@Ag@4-ATP, showing its strong SERS sensitizing ability. Notably, the superior SERS sensitizing ability of AuNS@Ag than that of AuNP@Ag is attributed to the hot-spot enhancement effect of polyhedral structure.

3.2. Construction of SCC-LFS for S. aureus assay

To verify the feasibility of SCC-LFS, a primer set targeting the *femA* gene of *S. aureus* was used for RPA amplification. More information on the amplicons was displayed in Fig. S1. Electrophoretic analysis of the amplification products was firstly presented in Fig. 3A. We intuitively observed that a bright target band (132 bp) appeared in lane 1 (amplicons) and no band appeared in lane 2 (blank control), indicating that the primer set was available. Besides, Cas9 and sgRNA alone did not impede amplicon migration (lane 3), whereas coexistence of them resulted in the disappearance of amplicon band (lane 4). This result is reasonable because amplicons bound to Cas9/sgRNA were blocked in the gel well, while Cas9 and sgRNA alone could not bind to amplicons. Therefore, the efficient binding of Cas9/sgRNA to amplicons was confirmed. As described in **Fig, 3B**, the positive group showed clear T-line and C-line, while the negative group showed only C-line. The corresponding SERS analysis in Fig. 3C showed that the Raman intensity of the positive group was 9 times that of the negative group, demonstrating that the method is available for *S. aureus* detection.

To demonstrate the sensitivity of SCC-LFS, various concentrations of *S. aureus* were tested. The images in Fig. 3D showed a concentration-dependent increase in T-line intensity over the range of 1–10^7 CFU/mL. The SERS analysis of the T-line in Fig. 3E–F revealed an acceptable linear relationship ($R^2 = 0.9827$) between Raman intensity and *S. aureus* concentration ranging from 10^0 to 10^5 CFU/mL. Considering that 1 CFU/mL of *S. aureus* was capable of inducing a visible T-line and a recognizable Raman signal, a limit of detection (LOD) of 1 CFU/mL was achieved. Compared to previous methods, SCC-LFS is superior in terms of sensitivity (Table S3), which is attributed to the strong SERS sensitizing ability of AuNS@Ag and the high amplification efficiency of RPA. More importantly, our method enables rapid on-site quantitative analysis with a smartphone-integrated portable Raman spectrometer, which is impractical for previous SERS-based LFSs relying on bulky instruments (Su et al., 2021). By incorporating a rapid extraction procedure (80 °C, 3 min), the entire assay could be completed in 45 min (Fig. S4), which is comparable or even superior to existing methods (Chen et al., 2020a; Shin et al., 2022; Yin et al., 2022).

The specificity of SCC-LFS was evaluated in Fig. 3G, revealing that SCC-LFS selectively produced a visible T-line and a distinguishable Raman signal in the presence of *S. aureus*, but did not respond to other pathogens. As depicted Fig. 3H, the Raman signal is slightly weakened with increasing storage time at room temperature (25 °C). Considering that the Raman signal of T-line remained almost unchanged after storage at 4 °C (Fig. S5), the method still has considerable potential for practical application. Subsequently, we performed five parallels with 10^3 and 0 CFU/mL of *S. aureus*, respectively (Fig. 3I). The relative standard deviations (RSDs) of the Raman intensity at 10^3 and 0 CFU/mL of *S. aureus* were 3.2% and 5.4%, respectively, indicating that SCC-LFS has a good reproducibility. The robustness of SCC-LFS was examined by testing *S. aureus*-spiked samples (Fig. S6), and a series of acceptable recoveries were obtained (Table S4). We then tested 36 elderly urine samples by SCC-LFS and gold standard culture method, respectively. As shown in Table S5, the results of SCC-LFS and culture method are in good agreement, indicating that SCC-LFS has a good accuracy. In addition, as a universal analytical method, SCC-LFS has also been successfully applied to the detection of *Mycoplasma pneumonia* (Fig. S7). We can find that no false positives were generated even in the presence of non-specific amplification, as the introduction of CRISPR/Cas9 helps to distinguish between target amplicons and by-products.

4. Conclusion

We have developed a dual-mode platform and applied it to the rapid and sensitive detection of *S. aureus*. This platform integrated the simplicity of visual readout and the quantitative capability of SERS, enabling the user to flexibly select the assay mode as needed. The method showed a LOD of 1 CFU/mL in both colorimetric and SERS modes, which is better than most existing methods. By incorporating a rapid extraction procedure, the entire assay can be completed in 45 min. Nevertheless, the current work is still limited by multi-step operations, which could be solved by creating an integrated module. In some cases, additional amplification steps may be difficult to implement in some cases, which could be addressed by developing new strategies that do not require pre-amplification. Additionally, the accuracy of the method should be validated with more real samples, which needs to be realized in our future work. In a nutshell, we hope that SCC-LFS can be developed as a routine tool for the detection of infectious pathogens.

CRediT authorship contribution statement

Junfeng Wang: Writing – original draft, Visualization, Validation, Software, Methodology, Investigation, Formal analysis, Data curation. **Han Jiang:** Writing – original draft, Visualization, Validation, Methodology, Investigation, Data curation. **Yuhong Chen:** Visualization, Validation, Supervision. **Xiaofan Zhu:** Visualization, Supervision. **Qian Wu:** Visualization, Validation, Supervision. **Wei Chen:** Writing – review & editing, Validation, Supervision. **Qihong Zhao:** Writing – review & editing, Supervision, Investigation. **Jie Wang:** Writing – review & editing, Validation, Supervision, Resources, Project administration. **Panzhu Qin:** Writing – review & editing, Writing – original draft, Validation, Supervision, Resources, Project administration, Methodology, Investigation, Funding acquisition, Formal analysis, Conceptualization.

Declaration of competing interest

The authors declare that they have no known competing financial interests or personal relationships that could have appeared to influence the work reported in this paper.

Data availability

Data will be made available on request.

Acknowledgements

This work was supported Anhui Provincial Natural Science Foundation (2308085QC112), University Natural Science Research Project of Anhui Province (KJ2021A0221), and Peak Discipline Construction Project in School of Public Health of Anhui Medical University in 2022–2023.

Appendix A. Supplementary data

Supplementary data to this article can be found online at https://doi.org/10.1016/j.bios.2024.116046.

References

Abbaspour, A., Norouz-Sarvestani, F., Noori, A., Soltani, N., 2015. Biosens. Bioelectron. 68, 149–155.
Bai, A.D., Lo, C.K.L., Komorowski, A.S., Suresh, M., Guo, K., Garg, A., Tandon, P., Senecal, J., Del Corpo, O., Stefanova, I., Fogarty, C., Butler-Laporte, G., McDonald, E. G., Cheng, M.P., Morris, A.M., Loeb, M., Lee, T.C., 2022. Clin. Microbiol. Infect. 28 (8), 1076–1084.
Balderston, S., Taulbee, J.J., Celaya, E., Fung, K., Jiao, A., Smith, K., Hajian, R., Gasiunas, G., Kutanovas, S., Kim, D., Parkinson, J., Dickerson, K., Ripoll, J.-J., Peytavi, R., Lu, H.-W., Barron, F., Goldsmith, B.R., Collins, P.G., Conboy, I.M., Siksnys, V., Aran, K., 2021. Nat. Biomed. Eng. 5 (7), 713–725.
Cesewski, E., Johnson, B.N., 2020. Biosens. Bioelectron. 159, 112214.
Chen, D., Ning, P., Zhang, Y., Jing, J., Zhang, M., Zhang, L., Huang, J., He, X., Fu, T., Song, Z., He, G., Qian, D., Zhu, X., 2020a. ACS Appl. Mater. Interfaces 12 (17), 20138–20144.
Chen, Q., Tian, T., Xiong, E., Wang, P., Zhou, X., 2020b. Anal. Chem. 92 (1), 573–577.
Cheng, X., Yang, X., Tu, Z., Rong, Z., Wang, C., Wang, S., 2023. J. Hazard Mater. 459, 132192.
Dong, T., Zhang, X., Yuan, J., Lin, Z., Yin, P., Yu, H., Wang, M., Liu, A., 2023. Anal. Chem. 95 (33), 12532–12540.
Fu, X., Sun, J., Liang, R., Guo, H., Wang, L., Sun, X., 2021. Trends Food Sci. Technol. 116, 115–129.
Jiang, H., Wu, Q., Zhao, Q., Liu, K., Bo, Q., Qin, X., Yan, C., Huang, L., Chen, W., Qin, P., 2023. Sensor. Actuator. B Chem. 396, 134581.
Li, J., Liang, P., Zhao, T., Guo, G., Zhu, J., Wen, C., Zeng, J., 2023. Anal. Bioanal. Chem. 415 (4), 545–554.
Liang, P., Guo, Q., Zhao, T., Wen, C.-Y., Tian, Z., Shang, Y., Xing, J., Jiang, Y., Zeng, J., 2022. Anal. Chem. 94 (23), 8466–8473.
Lu, Y., Yang, H., Bai, J., He, Q., Deng, R., 2022. Crit. Rev. Food Sci. Nutr. 1–21.
Monga, A., Pal, B., 2015. New J. Chem. 39 (1), 304–313.
Preechakasedkit, P., Panphut, W., Lomae, A., Wonsawat, W., Citterio, D., Ruecha, N., 2023. Anal. Chem. 95 (37), 13904–13912.
Sena-Torralba, A., Álvarez-Diduk, R., Parolo, C., Piper, A., Merkoçi, A., 2022. Chem. Rev. 122 (18), 14881–14910.
Shin, J., Yoon, T., Park, J., Park, K.S., 2022. Sensor. Actuator. B Chem. 365, 131871.
Su, L., Hu, H., Tian, Y., Jia, C., Wang, L., Zhang, H., Wang, J., Zhang, D., 2021. Anal. Chem. 93 (23), 8362–8369.
Su, Q., Ma, X., Dong, J., Jiang, C., Qian, W., 2011. ACS Appl. Mater. Interfaces 3 (6), 1873–1879.
Surewaard, B.G.J., Deniset, J.F., Zemp, F.J., Amrein, M., Otto, M., Conly, J., Omri, A., Yates, R.M., Kubes, P., 2016. J. Exp. Med. 213 (7), 1141–1151.
Trinh, H.D., Yoon, S., 2022. ACS Appl. Nano Mater. 5 (4), 5087–5095.
Wang, H., Wu, Q., Yan, C., Xu, J., Qin, X., Wang, J., Chen, W., Yao, L., Huang, L., Qin, P., 2022. Sensor. Actuator. B Chem. 369, 132293.
Wang, L., Wang, X., Cheng, L., Ding, S., Wang, G., Choo, J., Chen, L., 2021. Biosens. Bioelectron. 189, 113360.
Yan, J., Xu, Z., Zhou, H., Li, T., Du, X., Hu, R., Zhu, J., Ou, G., Li, Y., Yang, Y., 2022. Anal. Chem. 94 (47), 16481–16490.
Yin, M., Liu, C., Ge, R., Fang, Y., Wei, J., Chen, X., Chen, Q., Chen, X., 2022. Biosens. Bioelectron. 203, 114022.
Zhang, G., Hu, H., Deng, S., Xiao, X., Xiong, Y., Peng, J., Lai, W., 2023. Biosens. Bioelectron. 225, 115090.
Zhang, J., Tang, L., Yu, Q., Qiu, W., Li, K., Cheng, L., Zhang, T., Qian, L., Zhang, X., Liu, G., 2021a. Sensor. Actuator. B Chem. 344, 130325.
Zhang, Y., Wu, Y., Wu, Y., Chang, Y., Liu, M., 2021b. TrAC Trends Anal. Chem. 137, 116210.
Zhao, J., Wu, C., Zhai, L., Shi, X., Li, X., Weng, G., Zhu, J., Li, J., Zhao, J.-W., 2019. J. Mater. Chem. C 7 (27), 8432–8441.
Zhou, B., Ye, Q., Li, F., Xiang, X., Shang, Y., Wang, C., Shao, Y., Xue, L., Zhang, J., Wang, J., Ding, Y., Chen, M., Wu, Q., 2022a. Sensor. Actuator. B Chem. 351, 130906.
Zhou, S., Dong, J., Deng, L., Wang, G., Yang, M., Wang, Y., Huo, D., Hou, C., 2022b. ACS Sens. 7 (10), 3032–3040.
Zhu, R., Jiang, H., Li, C., Li, Y., Peng, M., Wang, J., Wu, Q., Yan, C., Bo, Q., Wang, J., Shen, C., Qin, P., 2023. Anal. Chim. Acta 1257, 341175.
Zhu, W., Wen, B.-Y., Jie, L.-J., Tian, X.-D., Yang, Z.-L., Radjenovic, P.M., Luo, S.-Y., Tian, Z.-Q., Li, J.-F., 2020. Biosens. Bioelectron. 154, 112067.